Laterally Inhomogeneous Melt Polymer Brushes. 1. Perturbation Analysis and General Predictions

Hai Tang

Departments of Materials Science and Engineering and of Chemistry and Materials Research Laboratory, University of Illinois, 1304 West Green Street, Urbana, Illinois 61801

Received February 28, 1995; Revised Manuscript Received May 30, 1995[⊗]

ABSTRACT: The classical limit self-consistent field theory of laterally homogeneous polymer brushes is generalized to laterally inhomogeneous melt systems, without imposing the Alexander–de Gennes approximation. This enables the appropriate description of the chain end distribution and confirmations, based on which the free energy expansion is obtained. The brushes are found to be always stable against height fluctuations. For grafted polymers, the equilibrium height profile and the height fluctuation spectrum strongly depend on the lateral wave vector q and the average surface coverage $\bar{\sigma}$. The structure factor (especially at large q) is qualitatively different from existing predictions by Fredrickson *et al.* and by Solis and Pickett based on the Alexander–de Gennes approximation, the latter of which even leads to lateral instability at small surface tension and/or large surface coverage, which is clearly an artifact of the approximation. For tethered polymers with lateral mobility, the height fluctuations exhibit a peak at $q = 0$ and a correlation length $\propto N^{1/2}\bar{\sigma}^{-1/2}$ (N being the polymerization index), whereas the surface coverage fluctuations are dominant over length scales $\sim N^{1/2}l$ (l being the statistical segment length). The fluctuations of the two quantities are correlated at small q, but are decoupled at large q.

I. Introduction

Polymers with one end tethered to a surface form dense layers, or "brushes" (see Figure 1), at sufficiently high surface coverage (number of chains per unit area).[1,2] Such materials include ordered phases and micelles assembled by block copolymers and polymers adsorbed on surfaces and interfaces. The end confinement and mutual exclusion force the chains to strongly stretch perpendicular to the tethering surfaces. The structure and thermodynamics of polymer brushes are successfully described by self-consistent field[3–6] and scaling theories.[7,8]

Most existing theoretical work is restricted to laterally homogeneous brushes. However, many factors, such as roughness and heterogeneity of the tethering surfaces, boundary effects, and nonuniform surface coverage, may give rise to lateral inhomogeneity. For instance, block copolymer surfaces often contain "islands" and "holes".[9] These issues are of both practical and scientific importance. Recent studies by computer simulations,[10,11] theories,[12–15] and experiments[16] demonstrate cluster formation in grafted polymers in poor solvents. As for melt polymer brushes, attempts within the Alexander–de Gennes approximation (assuming all chain ends are on the free surface)[7,8] have revealed fascinating effects arising from height fluctuations and mechanical deformation,[17,18] surface roughness,[18,19] insertion of guest objects,[20] etc. Although the Alexander–de Gennes approximation leads to good estimates for the free energy and height of laterally homogeneous brushes, it gives rise to the unphysical lateral instability of brushes,[18,19,21] due to the unrealistic assumption for the chain end distribution.

We generalize the classical limit self-consistent field for laterally *homogeneous* brushes[4,6] to laterally *inhomogeneous* melt systems. This corresponds to lifting the Alexander–de Gennes approximation in refs 17 and 18, which is shown to be essential for obtaining the correct chain end distribution and the free energy expansion

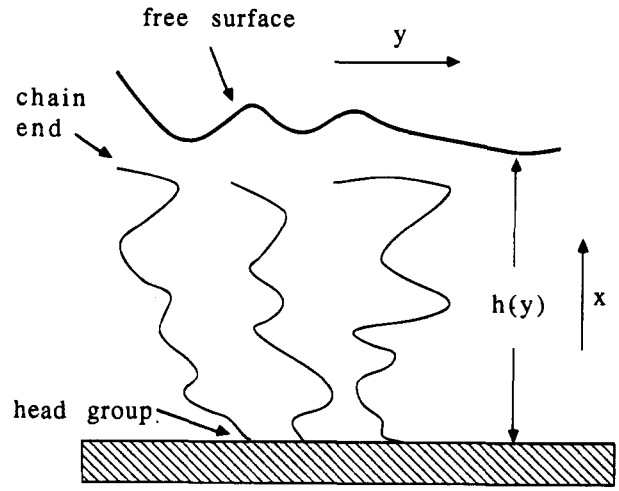

Figure 1. Schematic plot of a melt polymer brush with inhomogeneity in the y direction. The height of the brush is denoted by $h(y)$.

in terms of lateral inhogeneity. Studies within this approach will be presented in a series of publications. This first paper develops a perturbation analysis for brushes tethered on flat surfaces, based on which general predictions are make for the height profile, layer stability, and fluctuations. Section II provides a formal description of the generalized self-consistent field theory. Section III presents a perturbation analysis, which relates the laterally inhomogeneous surface coverage, height, chain end density, and the mean field potential and derives the free energy expansion. Grafted polymers are studied in section IV, where the equilibrium height profile and the structure factor for the height fluctuations are obtained. Tethered polymers with lateral mobility are investigated in section V, where the height and surface coverage fluctuations and their correlations are investigated. Further studies of the height (and surface coverage for chains with lateral mobility) profile(s), boundary effects, etc., and extension to rough tethering surfaces will appear in subsequent papers of the series.[22]

[⊗] Abstract published in *Advance ACS Abstracts,* August 1, 1995.

0024-9297/95/2228-6258$09.00/0

II. Formalism

Consider a brush composed of monodisperse polymers (each with N monomers at $x > 0$) end-tethered on a flat surface at $x = 0$ (see Figure 1). The brush is characterized by the surface coverage $\sigma(\boldsymbol{\varrho})$ [$\boldsymbol{\varrho} = (y, z)$], the height $h(\boldsymbol{\varrho})$, the local monomer volume fraction $\phi(\mathbf{r})$, and the end density $\eta(\mathbf{r})$, which are related by

$$\frac{1}{N\nu}\int d\boldsymbol{\varrho}\int_0^{h(\boldsymbol{\varrho})} dx\ \phi(\mathbf{r}) = \int d\boldsymbol{\varrho}\ \sigma(\boldsymbol{\varrho}) = \int d\boldsymbol{\varrho}\int_0^{h(\boldsymbol{\varrho})} dx\ \eta(\mathbf{r}) \tag{2.1}$$

all giving the total number of chains, where ν is the monomer volume.

Suppose the τth monomer on the ith chain is located at $\mathbf{r}_i(\tau)$. The partition function of the brush is

$$Q = \int \prod_i D\mathbf{r}_i(\tau) e^{-\beta H} \tag{2.2}$$

subject to the surface and end confinement constraints $\mathbf{r}_i(\tau) \geq -$ and $x_i(N) = 0$. Here $\beta = 1/k_B T$, and the Edwards Hamiltonian is

$$\beta H = \sum_i \frac{3}{2l^2}\int_0^N d\tau \left|\frac{d\mathbf{r}_i}{d\tau}\right|^2 + V[\{\mathbf{r}_i(\tau)\}] \tag{2.3}$$

where l is the statistical segment length. The contour integrals account for the conformational entropy, and the potential V includes contributions from both monomer–monomer interactions and external forces. Within the mean field approximation, V only depends on the spatial location, i.e., $V = V(\mathbf{r})$, which is the mean field potential at $\mathbf{r}$ imposed by all the other monomers and external influences.

Minimizing the free energy $\beta F = -\ln Q$ yields the self-consistent field equations,[3,5] which may be solved numerically. For analytic tractability, we will restrict our attention to the long chain and strong stretching ($N^{1/2}l \ll h \ll Nl$) regime (or the classical limit), where the average of the contour integrals in eq 2.3 is much greater than 1, such that the distribution of chain configurations is sharply peaked around the most probable conformation (the "classical trajectory"),[4,6] i.e., one which minimizes H.

The classical trajectory corresponds to the path of a classical particle with mass $3/l^2$ in the potential $-V(\mathbf{r})$, when τ is interpreted as time.[6] The equation of motion is

$$\frac{3}{l^2}\frac{d^2\mathbf{r}}{d\tau^2} = \nabla V(\mathbf{r}) \tag{2.4}$$

with the initial and terminal (or "equal time") conditions

$$\left.\frac{d\mathbf{r}}{d\tau}\right|_{\tau=0} = 0 \tag{2.5}$$

$$x(\tau{=}N) = 0 \tag{2.6}$$

respectively. Equation 2.5 emerges as the chain end and is stress free. Integrating eq 2.4 subject to the initial condition in eq 2.5 produces

$$\frac{3}{2l^2}\left|\frac{d\mathbf{r}}{d\tau}\right|^2 = V[\mathbf{r}(\tau)] - V(\mathbf{r}_0) \tag{2.7}$$

where $\mathbf{r}_0 = \mathbf{r}(\tau = 0)$.

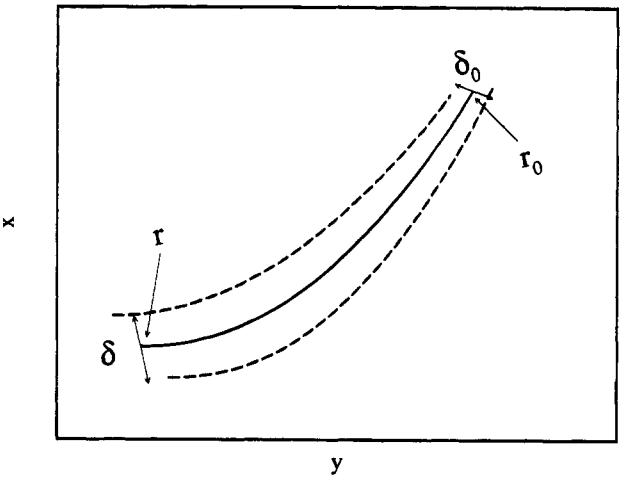

Figure 2. 2D plot of a set of classical paths which originate near $\mathbf{r}_0$ with a cross section of δ_0 and pass by $\mathbf{r}$ with a cross section of δ.

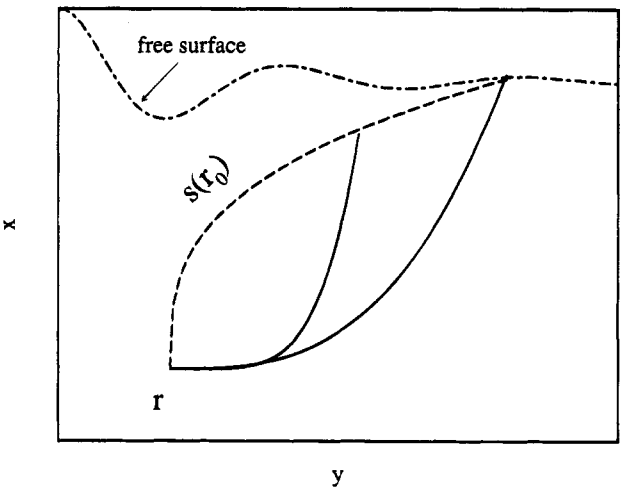

Figure 3. Origins of the classical paths passing through $\mathbf{r}$ (the solid curves) forming the dashed curve $S(\mathbf{r}_0)$.

The monomer concentration $\phi(\mathbf{r})$ and the surface coverage $\sigma(\boldsymbol{\varrho})$ are closely related to the chain end density $\eta(\mathbf{r})$ and the classical trajectories. For a set of paths which originate near $\mathbf{r}_0$ and pass by $\mathbf{r}$ (the 2D version is plotted in Figure 2), the cross section of the trajectories is initially δ_0, but becomes δ near $\mathbf{r}$. Therefore, the concentration at $\mathbf{r}$ contributed by polymers with ends at $\mathbf{r}_0$ is

$$\eta(\mathbf{r}_0)\nu\frac{\delta_0 d\tau}{\delta|d\mathbf{r}|} = \frac{\eta(\mathbf{r}_0)\nu}{|d\mathbf{r}/d\tau|}\frac{\delta_0}{\delta} \tag{2.8}$$

where $|d\mathbf{r}/d\tau|$ is given by the equation of motion in eq 2.7. On the other hand, as shown in Figure 3, paths (the solid curves) originating from any point on the line $s(\mathbf{r}_0)$ (the dashed curve extending from $\mathbf{r}$ to the free surface) go through $\mathbf{r}$. Therefore, the total concentration at $\mathbf{r}$ is obtained by integrating eq 2.8 along $s(\mathbf{r}_0)$ as

$$\phi(\mathbf{r}) = \nu\int ds\frac{\eta(\mathbf{r}_0)}{|d\mathbf{r}/d\tau|}\frac{\delta_0}{\delta} = \int ds\frac{\eta(\mathbf{r}_0)}{\sqrt{\frac{2l^2}{3}[V(\mathbf{r}) - V(\mathbf{r}_0)]}}\frac{\delta_0}{\delta} \tag{2.9}$$

where eq 2.7 has been inserted.

Likewise, the surface coverage is deduced by considering $\mathbf{r} = (x=0, \boldsymbol{\varrho})$. The trajectories initiating within the cross section of δ_0 near $\mathbf{r}_0$ terminate in an area of dy dz near $(0, \boldsymbol{\varrho})$. Therefore,

$$\sigma(\boldsymbol{\varrho}) = \int ds\, \eta(\mathbf{r}_0)\frac{\delta_0}{dy dz} \tag{2.10}$$

We will only consider melt brushes for which the incompressibility constraint is adopted, i.e.,

$$\phi(\mathbf{r}) = \begin{cases} 1 & \text{if } 0 < x < h(\varrho) \\ 0 & \text{otherwise} \end{cases} \tag{2.11}$$

In grafted polymers, $\sigma(\boldsymbol{\varrho})$ is fixed, whereupon eq 2.9 provides a stringent constraint on the end density and the potential, whereas in tethered polymers with lateral mobility, $\sigma(\boldsymbol{\varrho})$ is a thermodynamic variable that minimizes the free energy at equilibrium.

The key to solving the problem is finding an appropriate potential $V(\mathbf{r})$. An elegant example is the theory for laterally homogeneous brushes.[4,6] The following perturbation calculations for brushes with weak laterial inhomogeneity is also highly nontrival.

III. Perturbation Analysis

We first assume that there is no exclusion zone for chain ends; namely, $\eta(\mathbf{r}_0) > 0$ throughout the brush. This will be justified in section VI below. On the basis of this assumption, it may be shown that the potential has the form

$$V(\mathbf{r}) = Bx^2 - A(\boldsymbol{\varrho}) \tag{3.1}$$

where

$$B = \frac{3\pi^2}{8N^2l^2} \tag{3.2}$$

and $A(\boldsymbol{\varrho})$ depends on the height profile $h(\boldsymbol{\varrho})$ and the surface coverage $\sigma(\boldsymbol{\varrho})$. Due to the separation of variables in $V(\mathbf{r})$ of eq 3.1, the motion in the x direction is independent of that in the y and z directions. Therefore, the terminal condition in eq 2.6 is satisfied for any end location. On the other hand, at weak lateral inhomogeneity, eq 3.1 is proved in Appendix A to be also necessary to meet the terminal requirement.

Equation 3.1 is the basis of the following perturbation analysis. For simplicity, the lateral inhomogeneity is first taken to exist only in the y direction, such that $A = A(y)$. Straightforward extension to the general case of inhomogeneity in both the y and z directions is made at the end of this section. The equation of motion in eq 2.4 is solved as

$$x_0 = x \sec\left(\frac{\pi\tau}{2N}\right) \tag{3.3}$$

$$y_0 = y - \frac{l^2}{6}\frac{dA}{dy}\tau^2 + O[(dA/dy)^2] \tag{3.4}$$

Equation 3.4 is obtained by assuming the variation of dA/dy along the path is small, i.e. (from eq 3.4), $|dA/dy(y) - dA/dy(y_0)| = |d^2A/dy^2(y - y_0)| \le (N^2l^2/6)|d^2A/dy^2||dA/dy| \ll |dA/dy|$, or

$$\frac{N^2l^2}{6}\left|\frac{d^2A}{dy^2}\right| \ll 1 \tag{3.5}$$

We also assume that along the path, the lateral displacement $|y(\tau = N) - y_0| \sim N^2l^2|dA/dy|$ (according to eq 3.4) is much smaller than the vertical displacement x_0. Except for x_0 very close to 0 (see section VI below for discussion), $x_0 \sim \bar{h}$. Therefore, we obtain

$$N^2l^2\left|\frac{dA}{dy}\right| \ll \bar{h} \tag{3.6}$$

Equations 3.5 and 3.6 are converted into constraints on the variation of surface coverage and height below, which provide the criteria for the validity of the following perturbation calculations.

Under these assumptions, $|dy| \ll |dx|$, such that in eqs 2.9 and 2.10 and Figures 2 and 3, $\delta \approx dy\, dz$, $\delta_0 \approx dy_0\, dz$ (as $z = z_0$), $ds \approx dx_0$, $V(\mathbf{r}) - V(\mathbf{r}_0) \approx B(x^2 - x_0^2)$, and the line $s(x_0, y_0)$ terminates on the free surface at $(x_0, y_0) \approx [h(y), y]$. These approximations simplify eqs 2.9 and 2.10 to

$$\phi(\mathbf{r}) \approx \nu\int_t^1 dt_0 \frac{\eta(t_0,y_0)}{\sqrt{\frac{2l^2}{3}B(t_0^2 - t^2)}}\frac{\partial y_0}{\partial y} \approx \nu\int_t^1 dt_0 \frac{\eta(t_0,y_0)}{\sqrt{\frac{2l^2}{3}B(t_0^2 - t^2)}}\left(1 - \frac{l^2}{6}\frac{d^2A}{dy^2}\tau^2\right) \tag{3.7}$$

$$\sigma(y) = h(y)\int_0^1 dt_0\, \eta(t_0,y_0)\frac{\partial y_0}{\partial y} = h(y)\int_0^1 dt_0\, \eta(t_0,y_0)\left(1 - \frac{l^2}{6}\frac{d^2A}{dy^2}N^2\right) \tag{3.8}$$

where $t = x/h(y)$, $t_0 = x_0/h(y)$, $\eta(t_0,y_0) = \eta(x_0,y_0)$, and $\partial y_0/\partial y$ is evaluated from eq 3.4.

We may separate η into the leading contribution η_0 and a small correction η_1, i.e.,

$$\eta(t,y) = \eta_0(t,y) + \eta_1(t,y) \tag{3.9}$$

Hence, expanding $\eta(t_0,y_0)$ about $\eta(t_0,y)$ produces

$$\eta(t_0,y_0) \approx \eta_0(t_0,y) + \eta_1(t_0,y) + (y_0 - y)\frac{\partial}{\partial y}\eta_0(t_0,y) \approx \eta_0(t_0,y) + \eta_1(t_0,y) - \frac{l^2}{6}\frac{dA}{dy}\tau^2\frac{\partial}{\partial y}\eta_0(t_0,y) \tag{3.10}$$

where eq 3.4 has been used. Substituting eq 3.9 into eq 3.7 and separating the leading terms from the smaller perturbations give rise to

$$\nu\int_t^1 dt_0 \frac{\eta_0(t_0,y)}{\sqrt{\frac{2l^2}{3}B(t_0^2 - t^2)}} = \phi(\mathbf{r}) = \begin{cases} 1 & \text{if } 0 < t < 1 \\ 0 & \text{otherwise} \end{cases} \tag{3.11}$$

$$\int_t^1 \frac{dt_0}{\sqrt{\frac{2l^2}{3}B(t_0^2 - t^2)}}\left[\eta_1(t_0,y) - \frac{l^2}{6}\frac{dA}{dy}\tau^2\frac{\partial\eta_0}{\partial y}(t_0,y) - \frac{l^2}{6}\frac{d^2A}{dy^2}\tau^2\eta_0(t_0,y)\right] = 0 \tag{3.12}$$

where $\phi(\mathbf{r})$ is given by eq 2.11.

Equation 3.11 is an Abel integral equation, which is easily solved as[23]

$$\eta_0(t,y) = \frac{t}{N\nu\sqrt{1-t^2}} = \eta_0(t) \tag{3.13}$$

independent of y, or $\partial\eta_0/\partial y = 0$. In fact, this is simply the chain end density of a laterally uniform brush[6] with height $h(y)$. Hence, η_0 represents the homogeneous part of η.

Inserting eq 3.13 into eq 3.12 produces

$$\int_t^1 dt_0 \frac{\eta_1(t_0,y)}{\sqrt{t_0^2 - t^2}} = I(t)\frac{d^2A}{dy^2} \tag{3.14}$$

where

$$I(t) = \frac{l^2}{6}\int_t^1 dt_0 \frac{\eta_0(t_0)}{\sqrt{t_0^2 - t^2}}t^2 = \frac{2N^2l^2}{3\pi^2}\int_t^1 dt_0 \frac{\eta_0(t_0)}{\sqrt{t_0^2 - t^2}}\arccos^2(t/t_0) \tag{3.15}$$

with eq 3.3 substituted. Note that $I(t=1,y) = 0$. Equation 3.14 is also an Abel integral equation, which is solved as[23]

$$\eta_1(t,y) = -\frac{2t}{\pi}\frac{d^2A}{dy^2}\int_t^1 \frac{dt_0}{\sqrt{t_0^2 - t^2}}\frac{\partial I}{\partial t_0}(t_0) \tag{3.16}$$

Inserting eqs 3.10, 3.13, and 3.16 into eq 3.8 leads to

$$\sigma(y) \approx h(y)\int_0^1 dt\left[\eta_0(t)\left(1 - \frac{l^2}{6}\frac{d^2A}{dy^2}N^2\right) + \eta_1(t,y)\right] = \frac{h(y)}{N\nu}\left(1 - \frac{N^2l^2}{9}\frac{d^2A}{dy^2}\right) \tag{3.17}$$

where $\int_0^1 dt\ \eta_1(t,y)$ is evaluated in Appendix B. Equation 3.17 is rewritten and linearized as

$$\frac{d^2A}{dy^2} = \frac{9}{N^2l^2}\left[1 - N\nu\frac{\sigma(y)}{h(y)}\right] \approx \frac{9}{N^2l^2\bar{h}}[h(y) - N\nu\sigma(y)] \tag{3.18}$$

where "$\bar{g}$"denotes the spatial average of g and $\bar{h} = N\nu\bar{\sigma}$, derived from eqs 2.1 and 2.11, has been used. Thus, the inhomogeneous part of the potential is induced by the deviation of $h(y)$ from $N\nu\sigma(y)$. Equation 3.18 may be understood from the fact that polymer end-tethered in the region of a brush with $h(y) < N\nu\sigma(y)$ are forced by the packing constraint to stretch laterally out of the region. This requires the $A(y)$ to be convex, or $d^2A/dy^2 < 0$. Whereas the opposite is required if $h(y) > N\nu\sigma(y)$.

Substituting eq 3.18 into eqs 3.5 and 3.6 produces the criteria for the validity of our perturbation analysis,

$$|h(y) - N\nu\sigma(y)| \ll 2\bar{h}/3 \tag{3.19}$$

$$\left|\int dy\ [h(y) - N\nu\sigma(y)]\right| \ll \bar{h}^2 \tag{3.20}$$

Inserting eq 3.18 into eq 3.16 yields

$$\eta_1(t,y) = \frac{18t}{\pi N^2l^2\bar{h}}[N\nu\sigma(y) - h(y)]\int_t^1 \frac{dt_0}{\sqrt{t_0^2 - t^2}}\frac{\partial I}{\partial t_0}(t_0) \tag{3.21}$$

The integral in eq 3.21 is evaluated numerically. The response ratio $N\nu R_\eta(t) = N\nu\eta_1(t,y)\bar{h}/[N\nu\sigma(y) - h(y)]$ and $R_\eta(t)/\eta_0(t)$ are plotted as functions of $t = x/h(y)$ in Figure 4. The former vanishes at $t = 0$ and 1 and has a peak of 0.81 at $t = 0.14$ (much closer to the tethering surface than to the free surface), where the modification on the end density due to lateral inhomogeneity is the biggest. The latter, on the other hand, is a monotonically decreasing function of t and diverges in proportion to $t^{-1/2}$ as $t \to 0$. When $|\eta_1(t,y)/\eta_0(t)| \geq 1$, or $t \leq [N\nu\sigma(y) - h(y)]^2/\bar{h}^2$, the perturbation calculation for η in eqs 3.9–3.16 breaks down, and the unphysical prediction of $\eta < 0$ is obtained when $N\nu\sigma(y) > h(y)$ also holds. It is shown in section VI below that these problems only affect a thin layer of the brush near the tethering surface. This merely gives rise to negligible higher order corrections to the free energy expansion.

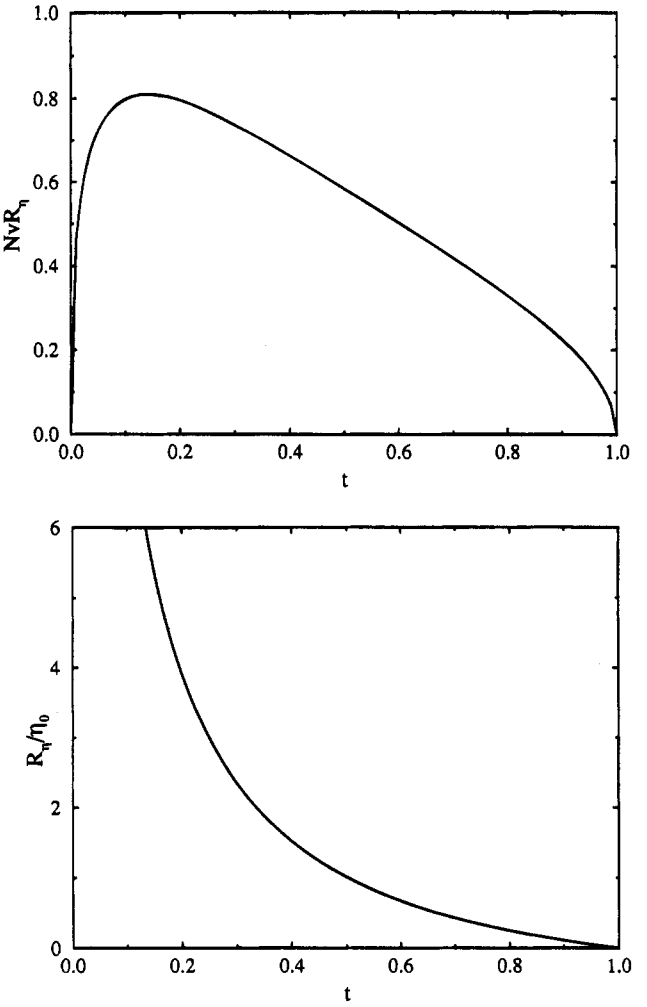

Figure 4. (a) Response ratio $N\nu R_\eta(t) = N\nu\eta_1(t,y)\bar{h}/[N\nu\sigma(y) - h(y)]$ and (b) $R_\eta(t)/\eta_0(t)$ as functions of $t = x/h(y)$.

We proceed to calculate the free energy of grafted polymers, which includes the chain elastic energy f_{el}, given by the contour integrals in eq 2.3, and the free surface tension γ, which is typically $(1-10)k_BT/l^2$. Extension to tethered polymers with lateral mobility is given in section V below. According to the Virial theorem,

$$\frac{3}{2l^2}\int_0^N d\tau\left(\frac{dx}{d\tau}\right)^2 = \int_0^N d\tau\, Bx^2(\tau) \tag{3.22}$$

due to the harmonic potential in x. Using eq 3.4, we also obtain

$$\frac{3}{2l^2}\int_0^N d\tau \left(\frac{dy}{d\tau}\right)^2 = \frac{l^2}{6}\left(\frac{dA}{dy}\right)^2 \int_0^N d\tau\, \tau^2 = \frac{N^3 l^2}{18}\left(\frac{dA}{dy}\right)^2 \quad (3.23)$$

The total free energy of the system is, therefore,

$$\beta F_{graft} = \int d\boldsymbol{\varrho} \int_0^{h(y)} dx\, \eta(x,y)\, f_{el}(x,y) + \beta\gamma \int d\boldsymbol{\varrho} \sqrt{1+\left(\frac{dh}{dy}\right)^2}$$

$$= \int d\varrho \int_0^{h(y)} dx \left[\frac{Bx^2}{\nu} + \frac{N^3 l^2}{18}\left(\frac{dA}{dy}\right)^2 \eta(x,y)\right] + \beta\gamma \int d\boldsymbol{\varrho} \sqrt{1+\left(\frac{dh}{dy}\right)^2} \quad (3.24)$$

$$\approx \int d\boldsymbol{\varrho} \left[\frac{\pi^2}{8N^2 l^2 \nu} h^3(y) + \frac{N^3 l^2 \bar{\sigma}}{18}\left(\frac{dA}{dy}\right)^2\right] + \beta\gamma \int d\boldsymbol{\varrho} \left[1 + \frac{1}{2}\left(\frac{dh}{dy}\right)^2\right] \quad (3.25)$$

where $\eta(x,y) \approx \eta_0(x,y)$ has been taken in the last step. Converting eq 3.25 into the Fourier space, retaining only quadratic terms, and generalizing to systems with inhomogeneity in both the y and z directions yield

$$\beta F_{graft} \approx \beta F^0_{graft} + \frac{1}{2}\sum_{\mathbf{q}\neq 0}\left\{\left(\frac{3\pi^2\bar{\sigma}}{4Nl^2} + \beta\gamma q^2\right) h(\mathbf{q})\, h(-\mathbf{q}) + \frac{9\bar{\sigma}}{Nl^2 q^2 \bar{h}^2}[h(\mathbf{q}) - N\nu\sigma(\mathbf{q})][h(-\mathbf{q}) - N\nu\sigma(-\mathbf{q})]\right\} \quad (3.26)$$

where

$$\beta F^0_{graft} = S\left(\frac{\pi^2 \bar{h}^3}{8N^2 l^2 \nu} + \beta\gamma\right) \quad (3.27)$$

with S being the total surface area, and the Fourier transform of eq 3.18 has been substituted.

IV. Grafted Polymers

The free energy of grafted polymers in eq 3.26 may be rewritten as

$$\beta F_{graft} = \beta \tilde{F}^0_{graft} + \frac{1}{2}\sum_{\mathbf{q}\neq 0} \mathbf{S}^{-1}_{graft}(q)[h(\mathbf{q}) - h_{eq}(\mathbf{q})][h(-\mathbf{q}) - h_{eq}(-\mathbf{q})] \quad (4.1)$$

where $\tilde{F}^0_{graft}$ equals F^0_{graft} plus contributions that only depend on the fixed $\sigma(\boldsymbol{\varrho})$, and

$$\mathbf{S}^{-1}_{graft}(q) = \frac{3\pi^2\bar{\sigma}}{4Nl^2}\left(1 + q^2\xi^2 + \frac{12}{\pi^2 q^2 \bar{h}^2}\right) \quad (4.2)$$

$$h_{eq}(\mathbf{q}) = \frac{N\nu\sigma(\mathbf{q})}{1 + \frac{\pi^2}{12} q^2 \bar{h}^2 (1 + q^2\xi^2)} \quad (4.3)$$

with

$$h_c = \left(\frac{4\beta\gamma l^2 \nu}{\pi^4}\right)^{1/3} N^{2/3} \quad (4.4)$$

$$\xi = \pi\left(\frac{h_c^3}{3\bar{h}}\right)^{1/2} \propto N^{1/2}\bar{\sigma}^{-1/2} \gg N^{1/2} l \quad (4.5)$$

As shown in section V, h_c is similar to the equilibrium height of polymer self-assemblies, such as block copolymer lamellae in the strong segregation limit. Minimizing the free energy in eq 4.1 gives $h_{eq}(\mathbf{q})$ as the Fourier transform of the equilibrium height profile of a free brush. Therefore, $S_{graft}(q)$ is the structure factor for the height fluctuations about the equilibrium profile. Since $S_{graft}(q) > 0$, the brush is always stable with respect to height fluctuations.

The structure factor in eq 4.2 resembles that of block copolymers,[23,24] an analogy also drawn in ref 13 between grafted polymers in solvents and block copolymers. This is due to the similarity between grafting and interblock connectivity. The q^2 term is the excess surface energy induced by height fluctuations with a correlation length ξ, whereas the q^{-2} part arises from the grafting constraint characterized by a scale $\sim\bar{h}$.

From eq 4.2, the peak wavevector and intensity of $S_{graft}(q)$ are

$$q^* = \frac{\sqrt{6}}{\pi}(h_c^3 \bar{h})^{-1/4} \propto N^{-3/4}\bar{\sigma}^{-1/4} \quad (4.6)$$

$$S^{-1}_{graft}(q^*) = \frac{3\pi^2\bar{\sigma}}{4Nl^2}[1 + 4(h_c/\bar{h})^{3/2}] \quad (4.7)$$

It follows from eq 4.6 that $q^* \ll N^{-1/2} l^{-1}$, which justifies taking the classical limit.

At relatively low surface coverage, or $\bar{h} \leq 2^{4/3} h_c$, the q dependent terms in eq 4.2 contribute significantly to the peak structure factor in eq 4.7. Hence, the peak width is roughly q^* ($\geq N^{-2/3} l^{-1}$), and the dominant fluctuations are on the length scales comparable to $2\pi/q^*$. Whereas at much higher surface coverage, or $\bar{h} \gg 2^{4/3} h_c$, the peak structure factor comes mainly from the q independent term in eq 4.2. Here, the peak spans over $2\sqrt{3}/(\pi\bar{h}) \leq q \leq \xi^{-1}$, where the lower (upper) bound is much smaller (larger) than q^*. Therefore, large fluctuations occur on a wide range of length scales. Figure 5 plots $(3\pi^2 h_c/4N^2 l^2 \nu) S_{graft}$ as a function of $q h_c$ for $\bar{h} = h_c$ and $10 h_c$, respectively, corresponding to the two scaling regimes just discussed. The numerical results are consistent with the analytic predictions.

When $(\pi^2/12) q^2 \bar{h}^2 (1 + q^2\xi^2) \ll 1$ or in the small q regime, eq 4.3 reduces to $h_{eq}(\mathbf{q}) \approx N\nu\sigma(\mathbf{q})$, or the height profile closely follows that of the surface coverage. Chain packing constraint requires lateral chain stretching to fill the space opened up or vacate the space closed out due to the difference between $h_{eq}(\mathbf{q})$ and $N\nu\sigma(\mathbf{q})$. This, however, is energetically costly at small q or large distances. On the other hand, for $(\pi^2/12) q^2 \bar{h}^2 (1 + q^2\xi^2) \gg 1$ or large q, eq 4.3 implies $h_{eq}(\bar{q}) \ll N\nu\sigma(\mathbf{q})$; i.e., the free surface hardly feels the inhomogeneity of the surface coverage. This is due to the fact that large q or small length scale roughness on the free surface sharply enhances the surface tension and, therefore, is unfavorable. When $\bar{h} \gg h_c$ (also implying $\bar{h} \gg \xi$), the peak width of the response is roughly $\bar{h}^{-1}$. Whereas if $\bar{h} \ll h_c$, or $\bar{h} \ll \xi$, the width is about $(\bar{h}\xi)^{-1/2} \propto N^{-3/4}\bar{\sigma}^{-1/4}$.

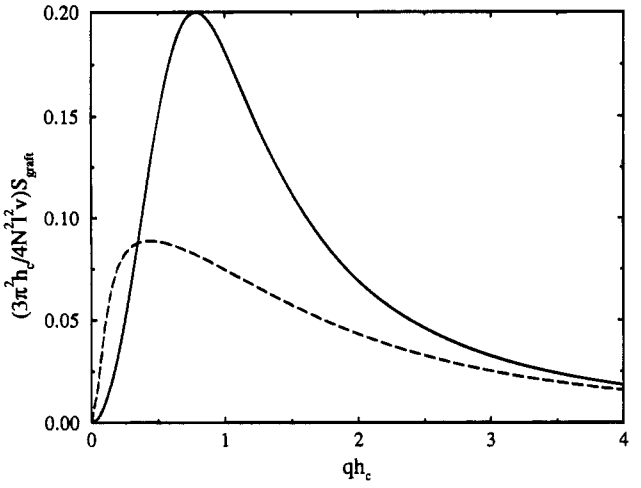

Figure 5. Reduced structure factor $(3\pi^2\bar{h}_c/4N^2\bar{l}^2\nu)S_{graft}$ for height fluctuations in grafted polymers as a function of qh_c. The solid and dashed curves are for $\bar{h} = h_c$ and $10h_c$, respectively.

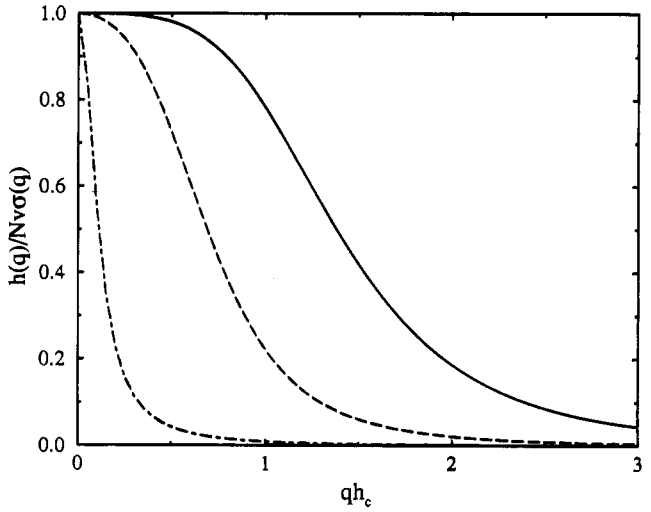

Figure 6. Response ratio $h(q)/N\nu\sigma(q)$ in grafted polymers as a function of qh_c. The solid, dashed, and dash-dotted curves are for $\bar{h} = 0.1h_c$, h_c, and $10h_c$, respectively.

As shown in Figure 6 for $\bar{h} = 0.1h_c$, h_c, and $10h_c$, respectively, the response ratio $h_{eq}(\mathbf{q})/N\nu\sigma(\mathbf{q})$ is a monotonically decreasing function of qh_c, which drops from 1 to 0. The response becomes weaker and its peak around $q = 0$ gets narrower with increasing average height (or surface coverage). Consistent with the discussion in the last paragraph, this indicates that the nonideal effects caused by inhomogeneous surface coverage are mostly "healed" on the free surface when the average surface coverage is high enough.

The special case of homogeneous surface coverage, i.e., $\sigma(\mathbf{q} \neq 0) = 0$, is also studied in refs 16 and 17 within the Alexander–de Gennes approximation. Their structure factor for the height fluctuations are both quantitatively and qualitatively different than that in eq 4.2. Indeed, all three approaches agree to within a constant prefactor at small q. For large q, however, apart from the same surface tension contribution, $\mathbf{S}^{-1}_{graft}(q)$ is independent of q in eq 3.26, but becomes positively and negatively proportional to q in refs 16 and 17, respectively. In fact, brushes are always stable according to ref 16, while ref 17 predits lateral instability in these systems if $\gamma < \gamma_c = 0.168k_BTN\nu^2\bar{\sigma}^3/l^2$. This condition may be realized at sufficiently high surface coverage. The instability is clearly unphysical, as chain packing introduces as effective repulsion among the strongly stretched polymers ($\bar{h} \gg N^{1/2}l$), which stabilizes the system. It remains to be resolved which, if any, of the two calculations is correct, and what is the cause of the instability. However, both have linear q terms that are important when γ is comparable to or smaller than γ_c. This, again, may be satisfied at high surface coverage. The discrepancies between the results in refs 16 and 17 and ours clearly demonstrate the limitations of the Alexander–de Gennes approximation.

V. Tethered Polymers with Lateral Mobility

Tethered polymers with lateral mobility have translational degrees of freedom parallel to the tethering surface plane. Therefore, the translational entropy $\sigma(\boldsymbol{\varrho}) \ln \sigma(\boldsymbol{\varrho})$ must be taken into account. In principle, we must also consider the effective interactions among head groups and the square gradient contributions $\propto|\nabla\sigma|^2$ arising from nonuniform $\sigma(\boldsymbol{\varrho})$. However, these effects are negligible for the long chains considered in this paper. Thus, the system free energy functional is

$$\beta F_{mobile} = \beta F_{graft} + \int d\boldsymbol{\varrho}\, \sigma(\boldsymbol{\varrho}) \ln \sigma(\boldsymbol{\varrho})$$

$$\approx \beta F^0_{mobile} + \frac{1}{2}\sum_{\mathbf{q}\neq 0}[\mathbf{S}^{-1}_{hh}(q)\, h(\mathbf{q})\, h(-\mathbf{q}) + 2\mathbf{S}^{-1}_{h\sigma}(q)\, h(\mathbf{q})\, \sigma(-\mathbf{q}) + \mathbf{S}^{-1}_{\sigma\sigma}(q)\, \sigma(\mathbf{q})\, \sigma(-\mathbf{q})] \quad (5.1)$$

where contributions beyond quadratic order have been dropped, F_{graft} is given by eq 3.26, and βF^0_{mobile} and elements of the inverse partial mmructure factor *matrix* $\mathbf{S}^{-1}(q)$ are given by

$$\beta F^0_{mobile} = \beta F^0_{graft} + S\bar{\sigma} \ln \bar{\sigma} = S\left(\frac{\pi^2\bar{h}^3}{8N^2\bar{l}^2\nu} + \beta\gamma + \bar{\sigma} \ln \bar{\sigma}\right) \quad (5.2)$$

$$\mathbf{S}^{-1}_{hh}(q) = S^{-1}_{graft}(q) \quad (5.3)$$

$$\mathbf{S}^{-1}_{h\sigma}(q) = -\frac{9}{Nl^2q^2\bar{h}} \quad (5.4)$$

$$\mathbf{S}^{-1}_{\sigma\sigma}(q) = \frac{1}{\bar{\sigma}} + \frac{9}{Nl^2q^2\bar{\sigma}} \quad (5.5)$$

$$\approx \frac{9}{Nl^2q^2\bar{\sigma}} \quad \text{for } q \ll N^{-1/2}l^{-1} \quad (5.6)$$

with $\mathbf{S}^{-1}_{graft}(q)$ given by eq 4.2.

An important class of brushes with lateral mobility are polymer self-assemblies (e.g., microdomains of strongly segregated block copolymers), where $\bar{\sigma}$ or $\bar{h}$ is allowed to vary, but the total number of polymers, or the total volume of the brush $S\bar{h}$, is fixed. The equilibrium height is obtained by minimizing the free energy in eq 5.2 at fixed $S\bar{h}$ as $\bar{h} = \pi^{2/3}h_c = 2.145h_c$, where h_c is given by eq 4.4.

A. Height and Surface Coverage Fluctuations. Inversion of the *matrix* $\mathbf{S}^{-1}$ yields the partial structure factors as

$$S_{hh}(q) = \mathbf{S}^{-1}_{\sigma\sigma}(q)/\det \mathbf{S}^{-1}(q) \quad (5.7)$$

$$S_{h\sigma}(q) = -\mathbf{S}^{-1}_{h\sigma}(q)/\det \mathbf{S}^{-1}(q) \quad (5.8)$$

$$S_{\sigma\sigma}(q) = \mathbf{S}^{-1}_{hh}(q)/\det \mathbf{S}^{-1}(q) \quad (5.9)$$

where eqs 4.2 and 5.3–5.5 may be used to yield

$$\det \mathbf{S}^{-1}(q) \equiv \mathbf{S}^{-1}_{hh}(q)\,\mathbf{S}^{-1}_{\sigma\sigma}(q) - [\mathbf{S}^{-1}_{h\sigma}(q)]^2$$

$$= \frac{\beta\gamma}{\bar{\sigma}}q^2 + \frac{9}{Nl^2}\left(\frac{\pi^2}{12} + \frac{\beta\gamma}{\bar{\sigma}}\right) + \frac{9}{Nl^2}\left(\frac{3\pi^2}{4Nl^2} + \frac{1}{\bar{h}^2}\right)q^{-2} \quad (5.10)$$

$$\approx \frac{27\pi^2}{4N^2l^4q^2}(1 + q^2\xi^2) \qquad \text{for } q \ll N^{-1/2}l^{-1} \quad (5.11)$$

Since $\det \mathbf{S}^{-1}(q) > 0$, the partial structure factors remain finite. Therefore, the system is always stable.

The peak of $S_{hh}(q)$ in eq 5.7 is found to be at $q = 0$, where the classical limit again applies. We restrict our attention to $q \ll N^{-1/2}l^{-1}$, where inserting eqs 5.6 and 5.11 into eq 5.7 produces

$$S_{hh}(q) \approx \frac{S_{hh}(0)}{1 + q^2\xi^2} \qquad \text{for } q \ll N^{-1/2}l^{-1} \quad (5.12)$$

with

$$S_{hh}(0) = \frac{4Nl^2}{3\pi^2\bar{\sigma}} \quad (5.13)$$

Therefore, ξ is the height–height correlation length. Figure 7 plots $S_{hh}(q,\bar{h})/S_{hh}(q=0,\bar{h}=h_c)$ as a function of qh_c for $\bar{h} = 0.5h_c$, h_c, and $2.145h_c$ (corresponding to self-assembled brushes), respectively. The peak becomes lower and broader with increasing average height (or surface coverage).

On the other hand, it may be shown by substituting eqs 4.2, 5.3, and 5.10 into eq 5.9 that $S_{\sigma\sigma}(q)$ approaches its maximum value of $\bar{\sigma}$ as $q \to \infty$ and saturates at $q \sim N^{-1/2}l^{-1}$, implying that the σ–σ correlation length is about $N^{1/2}l$. Of course, this is beyond the classical limit, where nonclassical effects must be taken into account.[26] For $q \ll N^{-1/2}l^{-1}$,

$$S_{\sigma\sigma}(q) \approx S_{\sigma\sigma}(0)\left(\frac{1}{1 + q^2\xi^2} + \frac{\pi^2}{12}q^2\bar{h}^2\right) \qquad \text{for } q \ll N^{-1/2}l^{-1} \quad (5.14)$$

where

$$S_{\sigma\sigma}(0) = \frac{\bar{\sigma}^2}{\bar{h}^2}S_{hh}(0) = \frac{4l^2}{3\pi^2\nu\bar{h}} \ll S_{\sigma\sigma}(q \gg N^{-1/2}l^{-1}) \approx \bar{\sigma} \quad (5.15)$$

From eq 5.14, a weak peak is obtained for $S_{\sigma\sigma}$ at $q = 0$ when $\bar{h} < (2\sqrt{3}/\pi)\xi$ or $\bar{h} < 2^{2/3}h_c = 1.59h_c$. Figure 8 shows $S_{\sigma\sigma}(q,\bar{h})/S_{\sigma\sigma}(q = 0, \bar{h} = h_c)$ as a function of qh_c in the small q region. A peak exists at $q = 0$ when $\bar{h} = h_c$ but is absent in self-assembled brushes with $\bar{h} = 2.145h_c$.

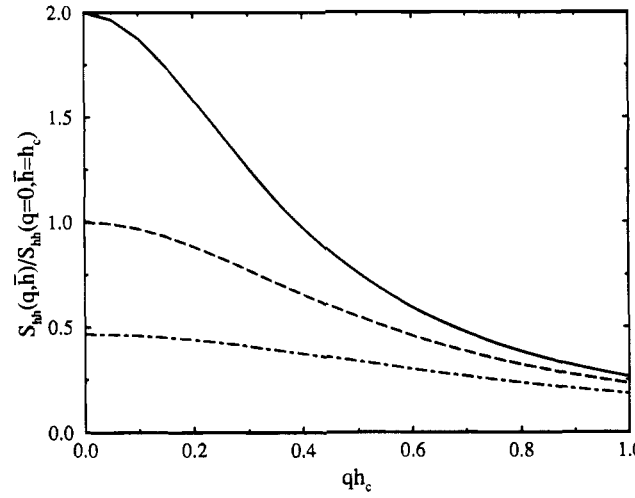

Figure 7. Reduced structure factor $S_{hh}(q,\bar{h})/S_{hh}(q = 0, \bar{h} = h_c)$ for height fluctuations in thethered polymers with lateral mobility. The solid, dashed, and dash-dotted curves are for $\bar{h} = 0.5h_c$, h_c, and $2.145h_c$ (corresponding to self-assembled brushes), respectively.

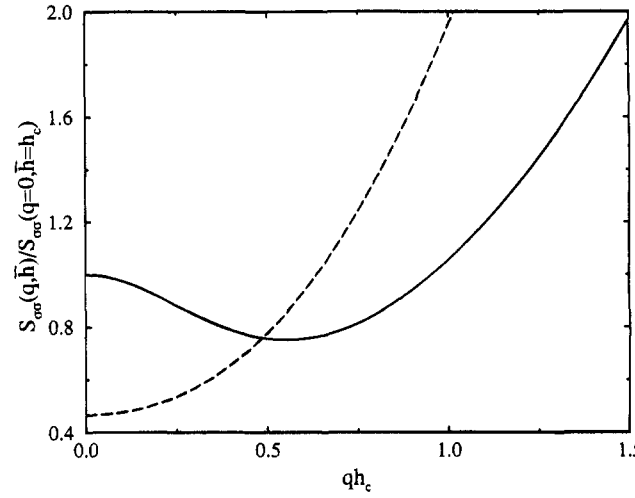

Figure 8. Reduced structure factor $S_{\sigma\sigma}(q,\bar{h})/S_{\sigma\sigma}(q = 0, \bar{h} = h_c)$ for surface coverage fluctuations in tethered polymers with lateral mobility. The solid and dashed curves are for $\bar{h} = h_c$ and $2.145h_c$ (corresponding to self-assembled brushes), respectively.

The different behavior between height and surface coverage fluctuations stems from the free surface tension. At small q, surface effect is negligible, therefore, the correlation between the h and σ fluctuations is easily established, as further demonstrated in the next subsection. For large q, however, the h fluctuations are severely suppressed by the surface tension, and the free surface is nearly flat, whereas the σ fluctuations are unaffected. In fact, they are the strongest at very large q, where chains are only slightly stretched. These results closely resemble the h–σ response of grafted polymers shown in section IV.

B. Collective Normal Modes. Due to the presence of the cross partial structure factor $S_{h\sigma}(q)$, the fluctuations in h and σ are correlated. The collective normal modes of these fluctuations may be understood by diagonalizing the free energy functional in eq 5.1 as

$$\beta F_{\text{mobile}} = \beta F^0_{\text{mobile}} + \frac{1}{2}\sum_{\mathbf{q}\neq 0}[\mathbf{S}_1^{-1}(q)\,u_1(\mathbf{q})\,u_1(-\mathbf{q}) + \mathbf{S}_2^{-1}(q)\,u_2(\mathbf{q})\,u_2(-\mathbf{q})] \quad (5.16)$$

where the normal modes $u_{1,2}(\mathbf{q})$ and the corresponding structure factors $S_{1,2}(q)$ are

$$\mathbf{S}_{1,2}^{-1}(q) + \frac{1}{2}[\mathbf{S}_{hh}^{-1}(q) + \mathbf{S}_{\sigma\sigma}^{-1}(q)/(N^2\nu^2)] \pm \frac{1}{2}\{[\mathbf{S}_{hh}^{-1}(q) + \mathbf{S}_{\sigma\sigma}^{-1}(q)/(N^2\nu^2)]^2 - 4 \det \mathbf{S}^{-1}(q)/(N^2\nu^2)\}^{1/2} \quad (5.17)$$

$$\theta = \arctan\left[N\nu\frac{\mathbf{S}_1^{-1}(q) - \mathbf{S}_{hh}^{-1}(q)}{\mathbf{S}_{h\sigma}^{-1}(q)}\right] \quad (5.18)$$

$$u_1(\mathbf{q}) = h(\mathbf{q}) \cos\theta + N\nu\sigma(\mathbf{q}) \sin\theta \quad (5.19)$$

$$u_2(\mathbf{q}) = -h(\mathbf{q}) \sin\theta + N\nu\sigma(\mathbf{q}) \cos\theta \quad (5.20)$$

Substituting eqs 4.2, 5.3, 5.4, 5.6, and 5.11 into eqs 5.17 and 5.18 yields

$$\mathbf{S}_{1,2}^{-1}(q) = \frac{9\bar{\sigma}}{Nl^2q^2\bar{h}^2}\left\{1 + \frac{\pi^2}{24}q^2\bar{h}^2(1 + q^2\xi^2) \pm \left[1 + \frac{\pi^4}{576}q^4\bar{h}^4(1 + q^2\xi^2)^2\right]^{1/2}\right\} \quad (5.21)$$

$$\theta = \arctan\left\{\frac{\pi^2}{24}q^2\bar{h}^2(1 + q^2\xi^3) - \left[1 + \frac{\pi^4}{576}q^4\bar{h}^4(1 + q^2\xi^2)^2\right]^{1/2}\right\} \quad (5.22)$$

When $(\pi^2/24)q^2\bar{h}^2(1 + q^2\xi^2) \ll 1$, eqs 5.19–5.22 reduce to $\theta \approx -\pi/4$, $u_{1,2}(\mathbf{q}) \approx [h(\mathbf{q}) \mp N\nu\sigma(\mathbf{q})]/\sqrt{2}$, and

$$S_2(q) \approx \frac{8Nl^2}{3\pi^2\bar{\sigma}(1 + q^2\xi^2)} \gg S_1(q) \approx \frac{Nl^2q^2\bar{h}^2}{18\bar{\sigma}} \quad (5.23)$$

Hence, at small q or large distances, the first normal mode is suppressed, i.e., $h(\mathbf{q}) \approx N\nu\sigma(\mathbf{q})$ or the height and surface coverage fluctuations are in phase. Otherwise, the packing constraint would require extending chains laterally over large distances, which is energetically costly.

Alternatively, if $(\pi^2/24)q^2\bar{h}^2(1+q^2\xi^2) \gg 1$, eqs 5.19–5.22 simplify to $\theta \approx 0$, $u_1(\mathbf{q}) \approx h(\mathbf{q})$, and $u_2(\mathbf{q}) \approx N\nu\sigma(\mathbf{q})$. Therefore, the height and surface coverage fluctuations are decoupled at large q or small length scales. The height fluctuations are suppressed by the surface tension.

Generally speaking, $-\tan\theta$ represents the degree of mixing of the height and surface coverage fluctuations in the normal modes. This is plotted in Figure 9 as a function of qh_c for $\bar{h} = 0.1h_c$, $2.145h_c$ (corresponding to self-assembled brushes), and $10h_c$, respectively. As qh_c increases from 0 to ∞, $-\tan\theta$ drops monotonically from 1 (h and σ fully correlated) to 0 (h and σ completely decoupled), as discussed above. Meanwhile, $-\tan\theta$ and its peak width are decreasing functions of the average height (or surface coverage). This indicates that the coupling between the height and surface coverage fluctuations may be tailored by adjusting the average surface coverage.

VI. Discussion and Conclusions

This section addresses several concerning issues encountered above, before concluding this paper.

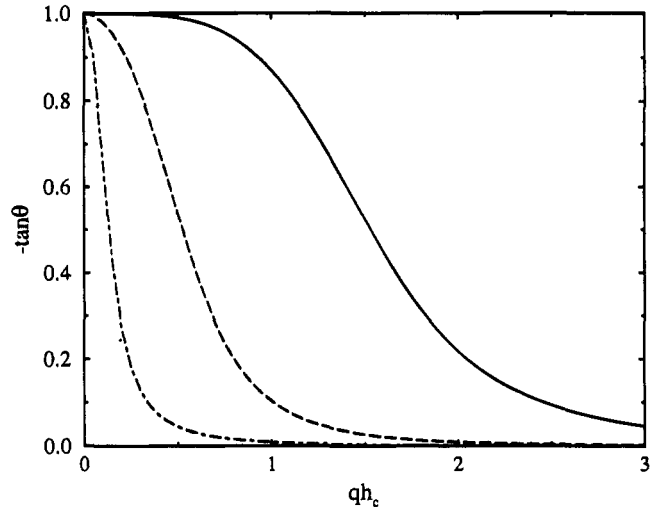

Figure 9. Degree of mixing $-\tan\theta$ of height and surface coverage fluctuations in the normal modes. The solid, dashed, and dash-dotted curves are for $\bar{h} = 0.1h_c$, $2.145h_c$ (corresponding to self-assembled brushes), and $10h_c$, respectively.

The most important issue is whether the chain end exclusion zone exists. As we know, the exclusion zone is present near convex tethering surfaces,[4,27] as monomers are expelled away from the tethering surface, where there is more space to be filled. This situation may also arise in laterally inhomogeneous brushes, even when the tethering surfaces are flat. As shown in Figure 2, chain ends in the area δ_0 are connected to head groups in the area $\delta(\tau = N)$. The ratio between them is obtained by substituting eq 3.18 into eq 3.8 as $\delta_0/\delta(\tau = N) \approx \partial y_0/\partial y(\tau = N) \approx 1 - (N^2l^2/6)\mathrm{d}^2A/\mathrm{d}y^2 \approx 1 + 3[N\nu\sigma(y) - h(y)]/(2\bar{h})$. When $N\nu\sigma(y) > h(y)$, $\delta_0/\delta(\tau = N) > 1$. Therefore, an exclusion zone is anticipated near such areas of the tethering surface. This is understandable, as chains tethered in these areas are forced to extend into surrounding areas. The thickness of the exclusion zone may be estimated in analogy to brushes tethered on convex surfaces[27] as $\bar{h}\exp\{-ch/[N\nu\sigma(y) - h(y)]\}$, where c is a constant of order 1 and $\bar{h}/[N\nu\sigma(y) - h(y)] \gg 1$ according to the criterion of weak lateral inhomogeneity in eq 3.19. Hence, the exclusion zone is exponentially thin and negligible in our analysis. In fact, even if the thickness of the exclusion zone is an appreciable fraction of the average brush height, neglecting it may only lead to tiny errors in the free energy.[27] Besides, chains with ends so close to the tethering surface are hardly stretched, so that the chain conformations are dominated by nonclassical rather than classical effects, and the classical limit description breaks down.

Another issue is the assumption that chain lateral displacement $|y(\tau = N) - y_0| \sim N^2l^2|\mathrm{d}A/\mathrm{d}y|$ (according to eq 3.4) is much smaller than the vertical displacement x_0, which certainly breaks down as the end location $x_0 \to 0$. Lifting this approximation should eliminate the negative end density η near the tethering surface obtained in eq 3.21, at least up to an exponentially thin layer near the tethering surface (see the preceding paragraph). In any case, these considerations mainly affect η very close to the tethering surface, while η elsewhere and the lateral part of the mean field potential A are only weakly perturbed. As long as the exclusion zone is negligible, eq 3.24 holds. Therefore, small corrections on η and A only lead to higher order contributions in the free energy expansion, which are ignored in our analysis.

Polydispersity is a complication always present in real polymer systems. It is found that the ends of longer chains tend to be excluded from the tethering surface,[28-30] which is closer to the Alexander–de Gennes description.[7,8] Thus, we speculate stronger height fluctuations and possible instability in polydisperse melt brushes. However, a sound assessment of the subject is not available due to technical difficulties associated with the presence of the exclusion zone.

In summary, we have generalized the classical limit self-consistent field theory of polymer brushes[4,6] to laterally inhomogeneous melt systems, which goes beyond the Alexander–de Gennes approximation.[7,8] An appropriate microscopic description of the brush structure is developed, based on which the free energy expansion is derived. The systems are shown to be always stable with respect to height fluctuations. For grafted polymers, the height profile and fluctuations are found to be sensitive to q and the average surface coverage. The structure factors (especially at large q) are qualitatively different from existing predictions[17,18] based on the Alexander–de Gennes approximation. In fact, ref 18 even predicts lateral instability at small surface tension and/or large surface coverage. These discrepancies are clearly artifacts of the approximation. For tethered polymers with lateral mobility, the height fluctuations have a peak at $q = 0$ and a correlation length $\xi \propto N^{1/2}\bar{\sigma}^{-1/2}$, whereas the surface coverage fluctuations are dominant over length scales $\sim N^{1/2}l$. Normal mode analysis yields that the height and surface coverage fluctuations are correlated at small q but are decoupled at large q. The work presented here should help us understand and tailor the lateral structure of melt polymer brushes.

Acknowledgment. I would like to express my gratitude toward Prof. Szleifer and Prof. Schweizer for encouragement and support. I also thank Prof. Witten and Dr. Li for enlightening discussion, Mr. Solis for pointing out several errors in the original manuscript and sending me ref 17 prior to publication, and anonymous referees for constructive suggests that help improved the manuscript.

Appendix A: Derivation of Eq 3.1

This appendix derives eq 3.1 for brushes with weak lateral inhomogeneity, assuming the absence of chain end exclusion zine (justified in section VI).

Consider a brush weakly inhomogeneous in the y direction with a periodicity of $2\pi/k$, where the magnitude of the inhomogeneity ϵ is small. The potential must have the general form

$$V(x,y) = V_0(x) + \epsilon V_1(x)\cos ky - O(\epsilon^2) \quad \text{(A1)}$$

According to eq A1, $\partial V/\partial y(y=n\pi/k) = 0$ holds through linear order in ϵ. Thus, particles released at rest from $y = n\pi/k$ do not move in the y direction; i.e., the motion becomes 1-dimensional, for which the terminal condition in eq 2.6 leads to

$$V(x,y=n\pi/k) = Bx^2 - A_n \quad \text{(A2)}$$

where B (given in eq 3.2) and A_n are constants.

Inserting eq A1 into eq A2 for $n = 0$ and 1 produces

$$V_0(x) + \epsilon V_1(x) = Bx^2 - A_0 \quad \text{(A3)}$$

$$V_0(x) - \epsilon V_1(x) = Bx^2 - A_1 \quad \text{(A4)}$$

Adding eq A4 to or subtracting eq A4 from eq A3 gives rise to

$$V_0(x) = Bx^2 - \frac{A_0 + A_1}{2} \quad \text{(A5)}$$

$$\epsilon V_1(x) = \frac{A_1 - A_0}{2} \quad \text{(A6)}$$

respectively. Substituting eqs A5 and A6 into eq A1 yields

$$V(x,y) = Bx^2 - \frac{A_0 + A_1}{2} + \frac{A_1 - A_0}{2}\cos ky + O(\epsilon^2) \quad \text{(A7)}$$

which, to linear order in ϵ, belongs to the class of potentials in eq 3.1.

Appendix B: Evaluation of $\int_0^1 dt\ \eta_1(t,y)$

This appendix evaluates the integral in eq 3.17,

$$J = \int_0^1 dt\ \eta_1(t,y) = -\frac{2}{\pi}\frac{d^2A}{dy^2}\int_0^1 t\,dt \int_t^1 \frac{dt_0}{\sqrt{t_0^2 - t^2}}\frac{\partial I}{\partial t_0}(t_0,y) \quad \text{(B1)}$$

where η_1 and I are given by eqs 3.16 and 3.15, respectively.

Altering the order of integration in eq B1 yields

$$J = -\frac{2}{\pi}\frac{d^2A}{dy^2}\int_0^1 dt_0 \frac{\partial I}{\partial t^0}(t_0,y)\int_0^{t_0}\frac{t\,dt}{\sqrt{t_0^2 - t^2}} = -\frac{2}{\pi}\frac{d^2A}{dy^2}\int_0^1 dt_0\, t_0 \frac{\partial I}{\partial t_0}(t_0,y) \quad \text{(B2)}$$

Changing the dummy variable t_0 in eq B2 to t, integrating by parts, and substituting eq 3.15 lead to

$$J = -\frac{2}{\pi}\frac{d^2A}{dy^2}\{[tI(t,y)]_{t=1} - [tI(t,y)]_{t=0} - \int_0^1 dt\, I(t,y)\} = \frac{4N^2l^2}{3\pi^3}\frac{d^2A}{dy^2}\int_0^1 dt \int_t^1 dt_0 \frac{\eta_0(t_0)}{\sqrt{t_0^2 - t^2}}\arccos^2(t/t_0) \quad \text{(B3)}$$

where $I(t=1,y) = 0$. Further altering the order of integration in eq B3 produces

$$J = \frac{4N^2l^2}{3\pi^3}\frac{d^2A}{dy^2}\int_0^1 dt_0\, \eta_0(t_0)\int_0^{t_0}\frac{dt}{\sqrt{t_0^2 - t^2}}\arccos^2(t/t_0) = \frac{N^2l^2}{18}\frac{d^2A}{dy^2}\int_0^1 dt_0\, \eta_0(t_0) = \frac{Nl^2}{18\nu}\frac{d^2A}{dy^2} \quad \text{(B4)}$$

where $\eta_0(t)$ is given by eq 3.13.

References and Notes

(1) Halperin, A.; Tirrell, M.; Lodge, T. P. *Adv. Polym. Sci.* **1991**, *100*, 31.

(2) Milner, S. T. *Science* **1991**, *251*, 905.
(3) Helfand, E. *Macromolecules* **1975**, *8*, 552. Helfand, E.; Wasserman, Z. R. *Macromolecules* **1976**, *9*, 879; **1978**, *11*, 960; **1980**, *13*, 994.
(4) Semenov, A. N. *Sov. Phys. JETP (Eng. Transl.)* **1985**, *61*, 733 [*Zh. Eksp, Teor. Fiz.* **1985**, *88*, 1242].
(5) Muthukumar, M.; Ho, J. S. *Macromolecules* **1989**, *22*, 965.
(6) Milner, S. T.; Witten, T. A.; Cates, M. E. *Europhys. Lett.* **1988**, *5*, 413; *Macromolecules* **1988**, *21*, 2610.
(7) Alexander, S. *J. Phys. (Paris)* **1977**, *38*, 983.
(8) de Gennes, P. G. *Macromolecules* **1980**, *13*, 1069.
(9) Menelle, A.; Russell, T. P.; Anastasiadis, S. H.; Satija, S. K.; Majkrzak, C. F. *Phys. Rev. Lett.* **1992**, *68*, 67.
(10) Lai, P.-Y.; Binder, K. *J. Chem. Phys.* **1992**, *97*, 586.
(11) Grest, G. S.; Murat, M. *Macromolecules* **1993**, *26*, 3108.
(12) Yeung, C.; Balazs, A. C.; Jasnow, D. *Macromolecules* **1993**, *26*, 1914.
(13) Williams, D. R. M. *J. Phys. II* **1993**, *3*, 1313.
(14) Tang, H.; Szleifer, I. *Europhys. Lett.* **1994**, *28*, 19.
(15) Soga, K. G.; Guo, H.; Zuckermann, M. J. *Europhys. Lett.* **1995**, *29*, 531.
(16) Zhao, W.; Krausch, G.; Rafailovich, M. H.; Sokolov, J. *Macromolecules* **1994**, *27*, 2933.
(17) Fredrickson, G. H.; Ajdari, A.; Leibler, L.; Carton, J.-P. *Macromolecules* **1992**, *25*, 2882.
(18) Solis, F. J.; Pickett, G. T. *Macromolecules* **1995**, *28*, 4307.
(19) Turner, M. S.; Joanny, J-F. *Macromolecules* **1992**, *25*, 6681.
(20) Williams, D. R. M.; Pincus, P. A. *Europhys. Lett.* **1993**, *24*, 29.
(21) Tang, H. *J. Chem. Phys.* **1993**, *99*, 1393.
(22) Tang, H. Manuscript in preparation.
(23) See, e.g.: Courant, R.; Hilbert, D. *Methods of Mathematical Physics*; Interscience: New York, 1953; Vol. 1.
(24) Leibler, L. *Macromolecules* **1980**, *13*, 1602.
(25) Ohta, T.; Kawasaki, K. *Macromolecules* **1986**, *19*, 2621.
(26) Marko, J. F.; Witten, T. A. *Phys. Rev. Lett.* **1991**, *66*, 1541.
(27) Ball, R. C.; Marko, J. F.; Milner, S. T.; Witten, T. A. *Macromolecules* **1991**, *24*, 693.
(28) Milner, S. T.; Witten, T. A.; Cates, M. E. *Macromolecules* **1989**, *22*, 853.
(29) Birshtein, T. M.; Liatskaya, Yu. V.; Zhulina, E. B. *Polymer* **1990**, *31*, 2185.
(30) Lai, P.-Y.; Zhulina, E. B. *Macromolecules* **1992**, *25*, 5201.

MA950257V